Advances in Geo-Energy Research

Vol. 7, No. 3, p. 176-188, 2023

Original article

A new semi-analytical flow model for multi-branch well testing in natural gas hydrates

Hongyang Chu[1,2,3]*, Jingxuan Zhang[1], Liwei Zhang[4,5], Tianbi Ma[4,6], Yubao Gao[1], W. John Lee[2]

[1]*School of Civil and Resources Engineering, University of Science and Technology Beijing, Beijing 100083, P. R. China*

[2]*Harold Vance Department of Petroleum Engineering, Texas A&M University, College Station 77843, USA*

[3]*State Key Laboratory of Petroleum Resources and Prospecting, China University of Petroleum, Beijing 102249, P. R. China*

[4]*Petroleum Exploration and Production Research Institute, SINOPEC, Beijing 100083, P. R. China*

[5]*School of Engineering, King's College, University of Aberdeen, Aberdeen AB24 3UE, UK*

[6]*Department of Geosciences, The University of Tulsa, Tulsa 74104, USA*

Keywords:
Natural gas hydrate
multi-branch well
flow regime
semi-analytical solution
stress-sensitive effects

Cited as:
Chu, H., Zhang, J., Zhang, L., Ma, T, Gao Y., Lee, W. J. A new semi-analytical flow model for multi-branch well testing in natural gas hydrates. Advances in Geo-Energy Research, 2023, 7(3): 176-188.
https://doi.org/10.46690/ager.2023.03.04

Abstract:
This paper presents a new semi-analytical solution and the related methodology to analyze the pressure behavior of multi-branch wells produced from natural gas hydrates. For constant bottom-hole pressure production, the transient flow solution is obtained by Laplace transforms. The interference among various branches is investigated using the superposition principle. A simplified form of the proposed model is validated using published analytical solutions. The complete flow profile can be divided into nine distinct regimes: wellbore storage and skin, vertical radial flow, linear flow, pseudo-radial flow, composite flow, dissociated flow, transitional flow, improvement flow and stress-sensitive flow. A well's multi-branch structure governs the vertical radial and the linear flow regimes. In our model, a dynamic interface divides the natural gas hydrates deposit into dissociated and non-dissociated regions. Natural gas hydrates formation properties govern the composite-effect, dissociated, transitional, and improvement flow regimes. A dissociation coefficient governs the difference in flow resistance between dissociated and non-dissociated natural gas hydrates regions. The dissociated-zone radius affects the timing of these flow regimes. Conversion of natural gas hydrates to natural gas becomes instantaneous as the dissociation coefficient increases. The pressure derivative exhibits the same features as a homogeneous formation. The natural gas hydrates parameter values in the Shenhu area of the South China Sea cause the prominent dissociated flow regime to conceal the later transitional and improvement flow regimes. Due to the maximum practical well-test duration limitation, the first five flow regimes (through composite flow) are more likely to appear in practice than later flow regimes.

1. Introduction

The goals of carbon neutrality and peak carbon production present urgent requirements for transitioning from traditional energy to clean energy sources (Hepburn et al., 2021; Chu et al., 2023). Clean energy sources include solar, hydrogen, wind, ocean, and geothermal (Dincer and Acar, 2015). Although clean energy has advantages in environmental protection, the current growth rate of these energy sources is far below target values. Fossil fuels accounted for 82% of the world's primary energy in 2015, and only a quarter of the world's electricity came from clean energy in 2017 (Gielen et al., 2019; Newell et al., 2019). Therefore, achieving efficient and large-scale clean energy production remains an elusive and unfulfilled goal. Natural gas hydrates (NGH) may assist.

The combustion products of NGH include only small amounts of CO_2 and water. Its energy density is enormous, with almost 164 cubic meters of methane per unit volume of

Yandy Scientific Press

*Corresponding author.
E-mail address: hongyangchu@126.com (H. Chu); m202110036@xs.ustb.edu.cn (J. Zhang); zhanglw.syky@sinopec.com (L. Zhang); matianbi.syky@sinopec.com (T. Ma); gyubao1996@163.com (Y. Gao); john-lee@tamu.edu (W. J. Lee).

Received December 10, 2022; revised December 31, 2022; accepted January 16, 2023; available online January 22, 2023.

hydrate structure. Thus, investigators have widely recognized NGH as a potential clean-energy source (Nair et al., 2018; Cai et al., 2020a, 2020b; Li et al., 2021; Shaibu et al., 2021; Nakajima et al., 2022). The accumulations in more than 230 NGH regions contain nearly 20,000 trillion cubic meters of methane gas. This amount is sufficient for centuries of energy needs (Kushwaha et al., 2019).

As a mature reservoir characterization method, well-testing technology has grown considerably over the decades, and it has achieved success in petroleum and natural gas evaluations (Lee, 1982; Lee et al., 2003; Spivey and Lee, 2013; He et al., 2017; Chu et al., 2022). Well testing begins as obtaining formation information by analyzing the pressure response caused by production changes. Evaluators can use the information from well tests to identify reservoir types, dominant parameters for wells and reservoirs, and reservoir pressure and reserves. Evaluators use type curves proposed by Gringarten and Bourdet extensively to analyze pressure transient responses (Gringarten et al., 1974; Bourdet et al., 1989). Further, to avoid production losses caused by shutting in wells for pressure buildup tests, evaluators can use production rate responses to obtain near-well and reservoir information (Blasingame et al., 1991; Blasingame and Lee, 1988). Lessons from the mature petroleum and gas industry show that well-testing technology is a prerequisite for efficiently developing oil and gas reservoirs.

Well-testing in NGH will require a mathematical fluid flow model in NGH accumulations. At present, proposed modeling approaches include analytical, semi-analytical, and numerical methods (Tsypkin, 2000; Sun et al., 2005; Tsimpanogiannis and Lichtner, 2007; Uddin et al., 2008; Myshakin et al., 2016; Hou et al., 2019; Roostaie and Leonenko, 2020; Xiao and Tian, 2020; Lu et al., 2022; Wei et al., 2022; Zhang et al., 2022). Numerical methods are good choices for describing the underground flow of NGH. Sun et al. (2005) proposed a one-dimensional numerical model. They investigated saturation, pressure, and temperature changes using finite-difference methods. Uddin et al. (2008) numerically simulated the kinetics and decomposition of NGH accumulations. Their kinetic model contains two mass transfer equations for gas, water, and NGH. Myshakin et al. (2016) forecasted NGH production performance in the Prudhoe Bay region using a commercial numerical simulator, CMG STARS. Results showed that inclined wells performed better than vertical wells. Hou et al. (2019) developed a numerical model to study the transient pressure behavior of vertical wells in class III hydrate reservoirs. Their model divided the reservoir into 16,100 grid blocks to capture the widely varying hydrate saturations, pressures, and temperatures near the wellbore. Using the open-source code HydrateResSim (HRS) developed by Lawrence Berkeley National Laboratory, Zhang et al. (2021, 2022) predicted the production performance of multi-branch wells in NGH reservoirs using the finite-element method. Using the commercial CMG STARS numerical simulator, Ye et al. (2022) clarified the effects of various well types and branch parameters on well productivity in NGH. Ye et al. (2023) studied gas production, temperature, and pressure behavior in a complex-structure NGH well in the Shenhu Sea area.

These numerical studies provide meaningful suggestions for numerical simulation and production forecasts in NGH. However, the demonstrated speed and accuracy of well-test type-curve matching leads many reservoir engineers to prefer the computational cost advantages of analytical or semi-analytical solutions. In an example analytical method study, Tsypkin et al. (2000) developed a mathematical model of gas production in NGH reservoirs with regions containing gas-water, gas-hydrate-water, and gas-hydrate. Hydrate dissociation always occurs in the gas-hydrate-water region. Hong et al. (2003) proposed an analytical production model for vertical wells in NGH. Production performance is controlled by heat transfer, fluid flow, and the kinetics of hydrate decomposition. Roostaie and Leonenko (2020) used an analytical method to couple the wellbore heating process and NGH dissociation in a coaxial vertical well. Their proposed analytical solution used a moving boundary to separate the dissociated and non-dissociated regions. Chen et al. (2022) proposed an analytical vertical well model in NGH reservoirs; the typical flow regimes are identified by pressure behavior. In summary, current analytical and semi-analytical models of NGH focus on vertical wells. A theoretical void remains for multi-branch wells with NGH decomposition and stress sensitivity.

We developed a semi-analytical multi-branch well model with NGH dissociation and stress sensitivity effects in this work. The Laplace transforms and the Stehfest numerical inversion algorithm are used to obtain point source solutions. The superposition principle allowed us to obtain the solution for a multi-branch well as the integral of the point source solution along each branch. The work is validated with the published analytical model. The essential parameters from multi-branch wells and NGH reservoirs are used for sensitivity analysis. A synthetic case study is performed using NGH properties from the Shenhu area in the South China Sea.

2. Methodology

2.1 Physical model and assumptions

Fig. 1 is a horizontal view of an infinite NGH reservoir. NGH dissociation causes two regions with different flow capabilities to appear. A multi-branch well is distributed in the center of the inner zone. The well uses depressurization to recover NGH: as the pressure decreases, the NGH begins to dissociate. The radius of the area with dissociated NGH is time-dependent. The size of the dissociated NGH zone increases with time. Other assumptions are as follows:

1) The dissociated NGH flow is single-phase compressible gas flow that satisfies Darcy's law.
2) Effects of gravity and capillary forces on gas flow are negligible.
3) Initial pressure distribution in the NGH is uniform.
4) NGH reservoir has impermeable top and bottom vertical boundaries.
5) The average permeability can replace permeability anisotropy in three dimensions, a theory Spivey and Lee (1998) proposed.

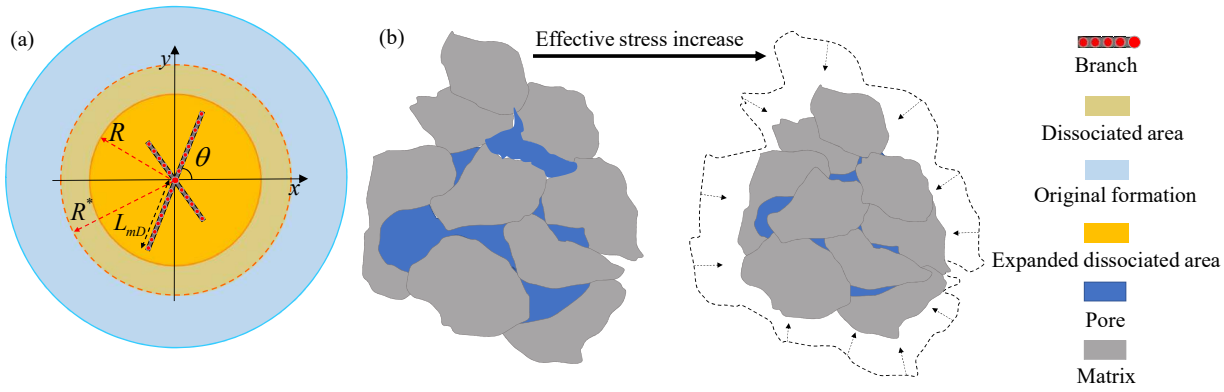

Fig. 1. Physical model of a multi-branch well with NGH dissociation and stress sensitivity. (a) Discrete multi-branch well with a moving interface and (b) pore shrinkage caused by stress sensitivity (modified from Wu et al. (2022)).

6) During NGH depressurization, effective stress increases due to the pore pressure decline. Stress-sensitive permeabilities are modeled by the Pedrosa (1986) method.

$$\alpha = \frac{1}{k}\frac{\partial k}{\partial p} \rightarrow k = k_i e^{-\alpha(p_i - p)} \tag{1}$$

where α is the permeability modulus, p is pressure, and k_i is the permeability at original pressure, p_i is the initial pressure.

2.2 Mathematical model

As NGH is recovered with a multi-branch well, the NGH reservoir can be divided into two regions. The governing equations of the dissociated zone and the un-dissociated zone are:

$$\begin{aligned}&\frac{3.6 p_i M_g k_i}{ZRT\mu r}\frac{\partial p_1}{\partial r} + \frac{3.6 p_i M_g k_i e^{-\alpha(p_i - p_1)}}{ZRT\mu}\left(\frac{\partial p_1}{\partial r}\right)^2 \\ &+ \frac{3.6 p_1 M_g k_i e^{-\alpha(p_i - p_1)}}{ZRT\mu}\frac{\partial^2 p_1}{\partial r^2} \\ &= \frac{\partial}{\partial t}\left\{\frac{p_1 M_g}{ZRT}\varphi\left[1 + C_H\left(p_1 - p_i\right)\right]\right\}\end{aligned} \tag{2}$$

$$\begin{aligned}&\frac{3.6}{r}\frac{\partial}{\partial r}\left(\frac{r p_2 M_g k_i e^{-\alpha(p_i - p_2)}}{ZRT\mu}\frac{\partial p_2}{\partial r}\right) \\ &= \eta^2\frac{\partial}{\partial t}\left\{\frac{p_2 M_g}{ZRT}\varphi\left[1 + C_H\left(p_2 - p_1\right)\right]\right\}\end{aligned} \tag{3}$$

where M_g is the gas molar mass, R is the gas-law constant, r is the radial distance, η refers to the $\sqrt{M_{12}/W_{12}}$, M_{12} is the mobility ratio, W_{12} refers to the diffusivity ratio, T is the temperature, C_H is the NGH compressibility, Z is the Z-factor, φ is the porosity, μ is the gas viscosity, and the subscripts 1 and 2 represent the inner and outer regions. As the multi-branch well starts to produce, the inner boundary conditions are:

$$\left(r\frac{\partial p_1}{\partial r}\right)_{r\rightarrow 0} = \frac{3.684\times 10^{-3} q_{sc}\mu B_H}{h k_i e^{-\alpha(p_i - p1)}} \tag{4}$$

where B_H is the formation volume factor of NGH, h is the reservoir thickness, and q_{sc} is the production rate at standard conditions. The NGH reservoir pressure at the infinite outer boundary is the initial formation pressure.

$$p_2\left(r\rightarrow\infty, t\right) = p_i \tag{5}$$

where the subscript i represents the initial state. The NGH reservoir has a uniform initial pressure distribution, as in Eq. (6):

$$p_i\left(r, 0\right) = p_2\left(r, 0\right) = p_i \tag{6}$$

For the moving interface caused by NGH dissociated effect, the pressure around the interface is:

$$p_1\left(R', t\right) = p_2\left(R', t\right) \tag{7}$$

where R' is the time-varying radius of the moving interface. With the dimensionless variables and pseudo pressure described in Appendix A, the mathematical model for the inner region is:

$$\frac{\partial^2\Psi_{1D}}{\partial r_D^2} + \frac{1}{r_D}\frac{\partial\Psi_{1D}}{\partial r_D} - \gamma_D\left(\frac{\partial\Psi_{1D}}{\partial r_D}\right)^2 = e^{\gamma_D\Psi_{1D}}\frac{\partial\Psi_{1D}}{\partial t_D} \tag{8}$$

where γ_D is the stress-sensitive permeability coefficient, Ψ_{1D} is dimensionless NGH pressure in the inner region, t_D is the dimensionless time, and r_D is the dimensionless distance. The dimensionless inner boundary and moving interface conditions can be expressed as:

$$\left(r_D e^{\gamma_D\Psi_{1D}\frac{\partial\Psi_{1D}}{\partial r_D}}\right)_{r_D\rightarrow 0} = -1 \tag{9}$$

$$\Psi_{1D}\left(R', t_D\right) = \Psi_{2D}\left(R', t_D\right) \tag{10}$$

The initial condition is:

$$\Psi_{1D}\left(r_D, 0\right) = \Psi_{2D}\left(r_D, 0\right) = 0 \tag{11}$$

Using Laplace transforms, and the Pedrosa substitution method (Pedrosa, 1986), the mathematical models for a dissociated region and an un-dissociated region are:

$$\frac{\partial^2 \bar{\xi}_{1D}}{\partial r_D^2}+\frac{1}{r_D}\frac{\partial \bar{\xi}_{1D}}{\partial r_D}=u\bar{\xi}_{1D} \tag{12}$$

$$\frac{\partial^2 \bar{\xi}_{2D}}{\partial r_D^2}+\frac{1}{r_D}\frac{\partial \bar{\xi}_{2D}}{\partial r_D}=\eta^2 u\bar{\xi}_{2D} \tag{13}$$

$$r_D\frac{\partial \bar{\xi}_{1D}}{\partial r_D}=-\frac{1}{u} \tag{14}$$

$$\bar{\xi}_{2D}\left(r_D\to\infty,u\right)=0 \tag{15}$$

$$\bar{\xi}_{1D}\left(R',u\right)=\bar{\xi}_{2D}\left(R',u\right) \tag{16}$$

where u is the Laplace variable, and ξ refers to the pressure after Pedrosa substitution. Following the works of Goel et al. (2001) and Chen et al. (2022), the time-varying distance of moving dissociated interface in an NGH reservoir is:

$$R'=2\sqrt{\frac{\lambda t_D k_i}{\varphi\mu C_H}} \tag{17}$$

where λ is the dissociation coefficient. The natural gas flow rate at the moving interface satisfies the equation:

$$\frac{\partial \bar{\xi}_{1D}}{\partial r_D}-\frac{1}{M_{12}}\frac{\partial \bar{\xi}_{2D}}{\partial r_D}=\frac{\lambda'_D}{\sqrt{u}}=\frac{\lambda'_D}{U} \tag{18}$$

where λ'_D is the improved NGH dissociated coefficient and U refers to $\sqrt{u}$.

$$\lambda'_D=2ZTS_H B_H\frac{k_i}{\mu_1}\frac{\pi h}{Bq_{sc}}\frac{p_{sc}}{T_{sc}C_H}\sqrt{3.6\pi\lambda} \tag{19}$$

where S_H is the NGH saturation, the subscript sc refers to the standard condition.

2.3 Solution strategy

Eq. (11) is a Bessel-type equation. Using the inner boundary condition in Eq. (14) and the dissociated interface condition in Eq. (16), we can write the final general solution in the dissociated region as:

$$\begin{aligned}\bar{\xi}_{1D}\left(r_D,u\right)=&\frac{VK_1\left(U\right)I_0\left(r_DU\right)+K_0\left(r_DU\right)I_1\left(U\right)}{I_1\left(U\right)-K_IK_1\left(U\right)}\\&-\frac{K_IK_0\left(r_DU\right)+I_0\left(r_DU\right)}{u^{1.5}\left[I_1\left(U\right)-K_IK_1\left(U\right)\right]}\end{aligned} \tag{20}$$

where K_1 is the first-order modified type II Bessel function, K_0 is the zero-order modified type II Bessel function, I_0 refers to the zero-order modified type I Bessel function, and I_1 is the first-order modified type I Bessel function. Similarly, Eqs. (13), (15), and (16) can be used to obtain the solution of an un-dissociated region.

$$\begin{aligned}\bar{\xi}_{2D}\left(r_D,u\right)=&\frac{K_0\left(r_DU\eta\right)V}{K_0\left(R'U\eta\right)\left[\left(I_1U\right)-K_IK_1U\right]}\\&\times\left[K_1\left(U\right)I_0\left(R'U\right)+K_0\left(R'U\right)I_1\left(U\right)\right.\\&\left.-\frac{1}{u^{1.5}}K_IK_0\left(R'U\right)+I_0\left(R'U\right)\right]\end{aligned} \tag{21}$$

where V can be given as:

$$V=\frac{M_{12}\lambda'_DK_0\left(R'U\eta\right)}{uM_{12}K_0\left(R'U\right)K_1\left(R'U\eta\right)\sqrt{\eta}-uM_{12}K_0\left(R'U\eta\right)K_1\left(R'U\right)} \tag{22}$$

K_I is defined as:

$$K_I=\frac{K_0\left(R'U\eta\right)I_1\left(R'U\right)+\frac{1}{M_{12}\eta I_0\left(R'U\right)K_1\left(R'U\eta\right)}}{K_0\left(R'U\eta\right)K_1\left(R'U\right)-\frac{1}{M_{12}\eta K_0\left(R'U\right)K_1\left(R'U\eta\right)}} \tag{23}$$

Because governing equations are linear, the superposition principle can be used to study the influence between various branch segments. Using pressure superposition and the line source function, the pressure response of the j^{th} segment on the i^{th} branch caused by the flow rate of the k^{th} segment in the lth branch is:

$$\bar{\xi}_{Dji}\left(r_D,u\right)=\sum_{l=1}^{m}\sum_{k=1}^{n}\bar{q}_{Dkl}\bar{\xi}_{1Dji} \tag{24}$$

where n is the number of segments on each branch and m is the number of branches. For constant rate production, the flow rate terms in a multi-branch well also satisfy the condition:

$$\sum_{l=1}^{m}\sum_{k=1}^{n}\bar{q}_{Dkl}=\frac{1}{u} \tag{25}$$

As Fig. 3 demonstrates, we can write Eqs. (24) and (25) for all segments in multi-branch well as:

$$A=\begin{bmatrix}a_{11} & \cdots & a_{1n} & 1 & \cdots & 0\\ a_{21} & \cdots & a_{1n} & 0 & 1 & 0\\ \cdots & \cdots & \cdots & \cdots & \cdots & \cdots\\ a_{n1} & \cdots & a_{nn} & 0 & 0 & 1\\ \cdots & \cdots & \cdots & \cdots & \cdots & \cdots\\ 0 & 0 & 0 & 1 & 1 & 1\end{bmatrix}_{(2N+1)\times(2N+1)} \tag{26}$$

where N refers to the total number of segments in a multi-branch well. The unknowns in Fig. 2 include the segments' flow rate term, pressure term, and BHP term from multi-branch well.

$$X=\begin{bmatrix}\bar{\xi}_{D,1} & \cdots & \bar{\xi}_{D,N} & \bar{q}_{D,1} & \cdots\bar{q}_{D,N} & \bar{\xi}_{wD}\end{bmatrix} \tag{27}$$

where $\bar{\xi}_{wD}$ is the BHP after Laplace transformation and Pedrosa substitution. For the BHP obtained, the Eq. (28) is used to add the effects of wellbore storage and skin factor (Van Everdingen and Hurst, 1949). The Stehfest numerical inversion algorithm is selected to convert the BHP in the Laplace domain to the BHP in the real domain (Stehfest, 1970).

$$\bar{\xi}_{wD}=\frac{S+u\bar{\xi}_{wD}\left(u\right)}{u\left\{1+C_Du\left[S+u\bar{\xi}_{wD}\left(u\right)\right]\right\}} \tag{28}$$

where C_D is the dimensionless wellbore storage coefficient and S is the skin factor. NGH dissociation leads to an increase in effective stress. Eq. (29) shows the effect of stress sensitivity on NGH reservoir permeability.

$$\Psi_{wD}\left(t_D\right)=-\frac{1}{\gamma_D}\ln\left[1-\gamma_D\times\xi_{wD}\left(t_D\right)\right] \tag{29}$$

For naturally-fractured porous media, the Laplace variable u can be replaced by $f(u)$ and our conclusions remain valid.

$$f(u)=\frac{\omega u(1-\omega)+\gamma}{u(1-\omega)+\gamma} \tag{30}$$

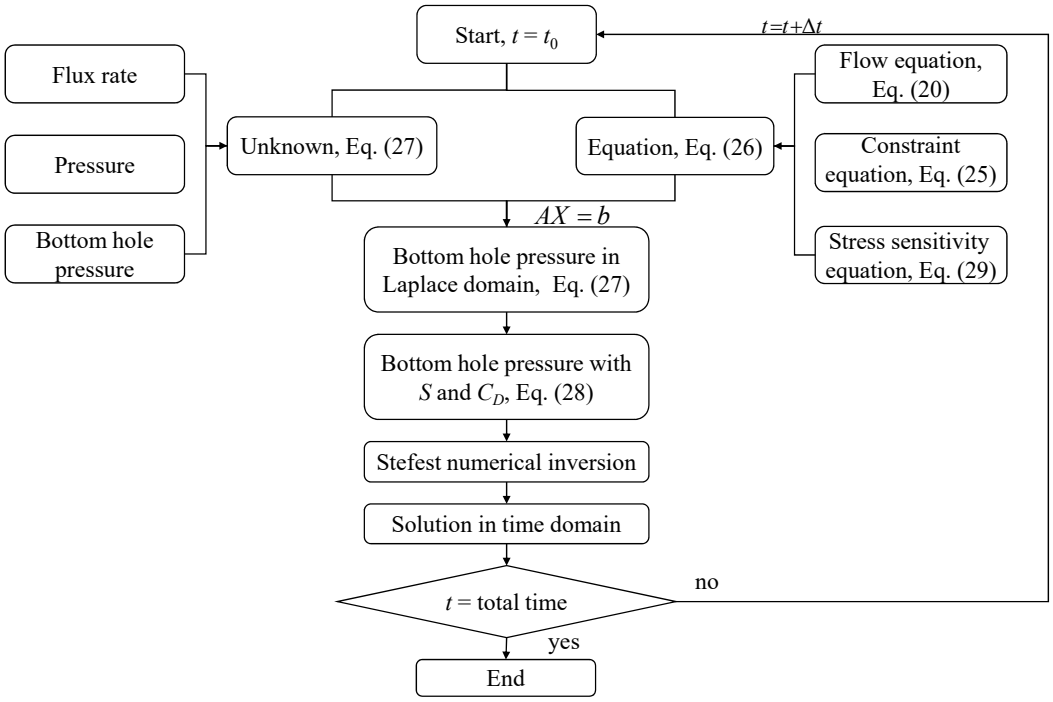

Fig. 2. Flow chart to obtain bottom-hole pressure for multi-branch well with NGH dissociation and permeability stress sensitivity.

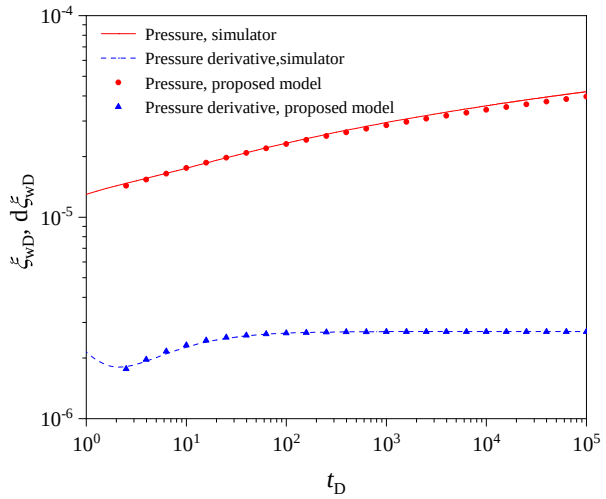

Fig. 3. Comparison of calculated pressures and derivatives from the simplified proposed model and the published analytical radially-composite model.

where γ is the inter-porosity flow factor and ω is the storativity ratio.

3. Method validation

By setting the branch length, dissociation coefficient, and permeability stress sensitivity coefficient in the model to small values, the proposed model simplifies to a radially- composite model for a vertical well. Thus, the analytical radial composite model of Ozkan and Raghavan (1991) is used to validate our proposed model. Table 1 provides the input parameters for model validation. The pressure data from the analytical model and the proposed model generated are plotted in a log-log coordinate system for comparison (Fig. 3). The comparison shows that the proposed model is reliable. The proposed model is semi-analytical and needs to be discretized only at the position of the multi-branch wellbore. This provides a significant advantage in computational cost because the matching process of well-test data requires hundreds of iterations using the model. The advantage of reduced computational cost makes the semi-analytical model especially suitable for well-test research.

4. Results and discussion

4.1 Complete flow regimes

Log-log plots of pressure and pressure derivative profiles from the proposed model (Fig. 4) help identify the typical flow regimes in NGH reservoirs. The parameter combinations in Table 1 are chosen to illustrate flow regimes more clearly. Well-test theory (Lee, 1982; Spivey and Lee, 2013) suggests nine possible flow regimes in NGH reservoirs as multi-branch wells produce NGH. Although Fig. 4 illustrates all nine flow regimes, factors such as test duration, reservoir heterogeneity, and decomposition coefficient may cause some flow regimes not to develop fully. Instead, some flow regimes may interact with one another and exhibit an integrated transitional flow feature.

(a) Wellbore-storage-effect regime.

NGH flows into the multi-branch wellbore as gas. Gas compressibility and wellbore volume cause differences in gas flow rate at the wellhead and the bottom of the well during the initial period of well testing. During this period, the pressure and derivative exhibit a straight line with a unit slope on a log-log plot.

Table 1. Model validation parameters for vertical well in NGH formation.

Parameter	Value	Unit
Initial pressure	30	MPa
Formation thickness	20	m
Permeability	5	md
Porosity	0.4	-
Total compressibility	0.0192	MPa^{-1}
Wellbore storage coefficient	3	m^3/MPa
Skin factor	1×10^{-5}	-
Composite radius	20	m
Mobility ratio	2	-
Dispersion ratio	2	-
Production rate	1	m^3/d

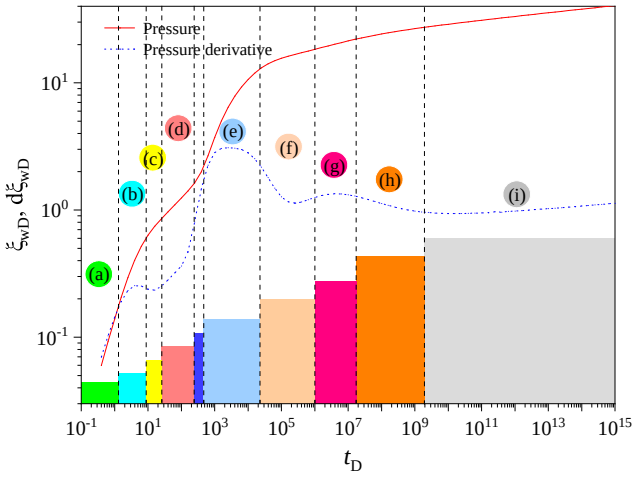

Fig. 4. Pressures and derivatives illustrate all flow regimes of a multi-branch well with dissociation and stress-sensitive effects in the NGH reservoir.

(b) Skin effect regime.

Contaminants, reservoir heterogeneities, and NGH dissociation cause an additional pressure drop as gas flows through the formation near the wellbore. This additional pressure drop is called the skin effect, and the derivative during this period increases with time.

(c) Vertical radial flow regime.

When the pressure response propagates from the initial horizontal direction to the vertical, the fluid in the three dimensional (3D) domain starts to flow into the multi-branch wellbore. In a slice in the z-direction in the 3D domain, the pressure response appears as a circle, and the circle's center is the wellbore (Fig. 5(a)).

(d) Linear flow regime.

As the pressure response spreads further, the gas beyond the wellbore begins to flow. Since the formation is effectively infinite in the horizontal direction, the fluid supply capacity in the horizontal direction is greater than in the vertical direction. Meanwhile, each branch in the multi-branch well can be simplified as a straight line. The gas flow direction at this time is perpendicular to the wellbore orientation in the 3D domain.

(e) Composite-effect flow regime.

The difference in flow resistance between the dissociated and original regions causes the pressure derivative to trend upward. The multi-branch well can be viewed as a point source compared to the dissociated region, and the gas flows to the wellbore in a pseudo-radial pattern.

(f) Dissociated flow regime.

The pressure response begins to propagate to the moving interface that dissociation causes. The NGH, at initial conditions, begins to dissociate in large quantities to form natural gas at this time. The flow capacity of dissociated natural gas is greatly enhanced, and gas begins to flow into the inner region, thus indicating the supply-boundary characteristics. The derivative decreases at this time.

(g) Transitional flow regime.

Although a large amount of NGH begins to dissociate into natural gas, the flow capacity in the un-dissociated region is still smaller than that of the inner region. Due to the difference in flow resistance difference between inner and outer regions, the pressure derivative turns upward.

(h) Improvement regime.

After NGH dissociation, pressure in the un-dissociated zone decreases. The physical properties of reservoir fluid begin to change from those of NGH to gas. The gas flow capacity from the outer region begins to increase gradually. The mobility and dispersion ratios tend to become uniform throughout the drainage area of the well. As a result, the pressure derivative begins to decrease.

(i) Stress-sensitive effect regime.

As flow continues, the pore pressure gradually decreases, and the effective stress increases. The permeability and porosity decrease as effective stress increases. The pressure derivative increases. Fluid flows radially to the multi-branch well (Fig. 5(b)) and can be regarded as a point source.

4.2 Sensitivity analysis

This section summarizes the results of a sensitivity analysis of production from NGH reservoirs with multi-branch wells. The model had two branches with a dimensionless branch length of 25. The dimensionless radius of the dissociated region was 100. The wellbore storage coefficient was 10, and the skin factor was 0.5. The basic mobility ratio was 3, and the dispersion ratio was 2. The dissociation coefficient was 1×10^{-4}.

(a)Effect of dissociation coefficient

The dissociation coefficient determines the dissociated volume of NGH per unit of time. Fig. 6 shows that the dissociation coefficient affects the composite-effect, dissociated, transitional, and improvement flow regimes. A small dissociation coefficient leads to a slower dissociation rate of NGH. At this point, the dissociated natural gas from the outer region begins to flow to the dissociation area, and the pressure derivative decreases. The transitional flow regime and the im-

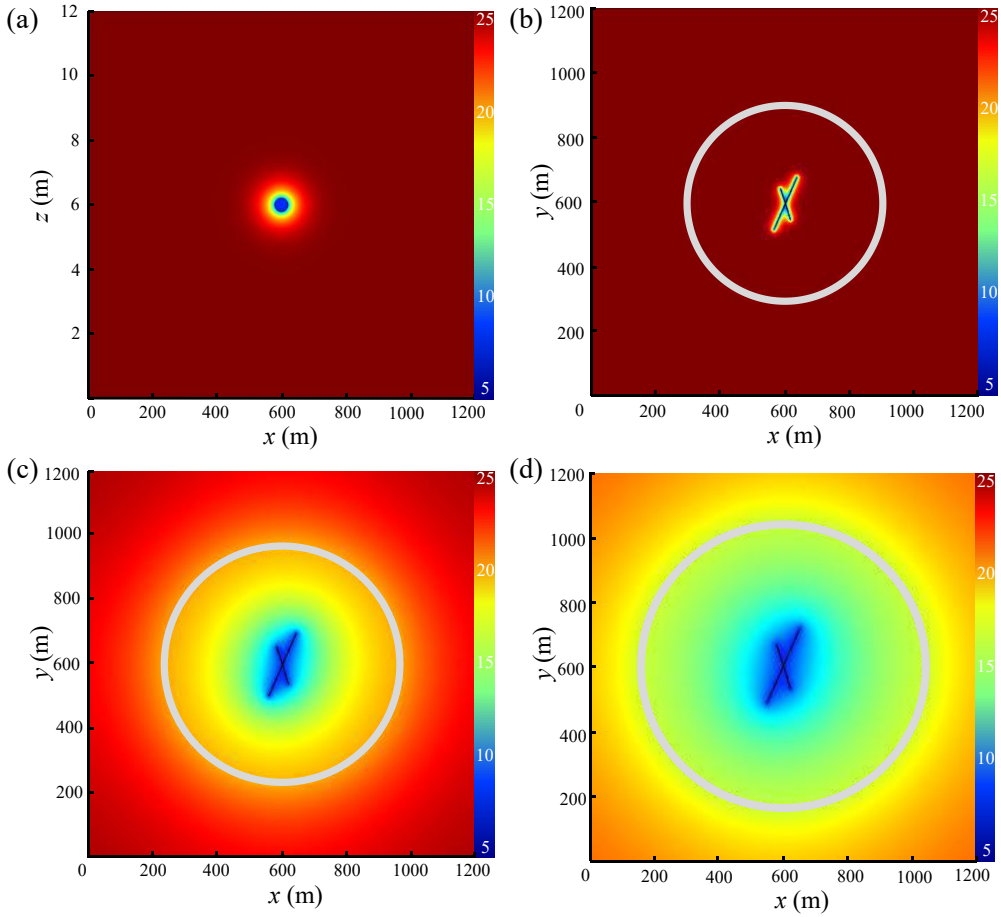

Fig. 5. Pressure distributions for a multi-branch well in an NGH reservoir during different flow regimes. (a) vertical radial flow regime, (b) linear flow regime, (c) composite-effect flow regime and (d) stress-sensitive effect regime.

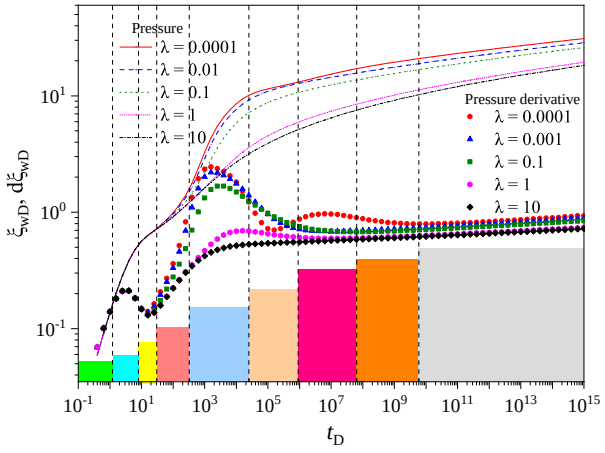

Fig. 6. Effect of dissociation coefficient on multi-branch well's pressure transient behavior.

provement regime caused by the composite feature appear next. As the NGH dissociation rate increases, derivatives curves gradually flatten. The formation exhibits homogeneous properties as the transformation of NGH to natural gas occurs instantaneously.

(b)Effect of the radius of the dissociated region

Fig. 7 shows that the radius of the dissociated region is related to the start times of the composite-effect, dissociated, transitional, and improvement flow regimes. When the radius of the dissociated region increases to 1,000, the multi-branch well can be regarded as a point source, and the fluid flow around the well can also exhibit radial flow characteristics. The starting and ending times of these flow regimes are proportional to the radius of the dissociated area, but the pressure derivative value is independent of the radius. Meanwhile, the durations of these flow regimes are prolonged as the radius increases.

(c)Effect of branch angle

Fig. 8 shows that branch angle variation affects the vertical radial and linear flow regimes. The branch angle does not affect the wellbore storage and skin effect flow regimes as the pressure response spreads around a single discrete segment. When the pressure response propagates, the impact of individual branch segments emerges. Derivatives during vertical radial and linear flow regimes correlate positively with the branch angle. Derivative behavior changes are influenced by branch angle peaks in the vertical radial flow regime and disappear in the later linear flow regime. The effect of branch angle on the pressure derivative shows that a multi-branch well structure controls the vertical radial and linear flow regimes.

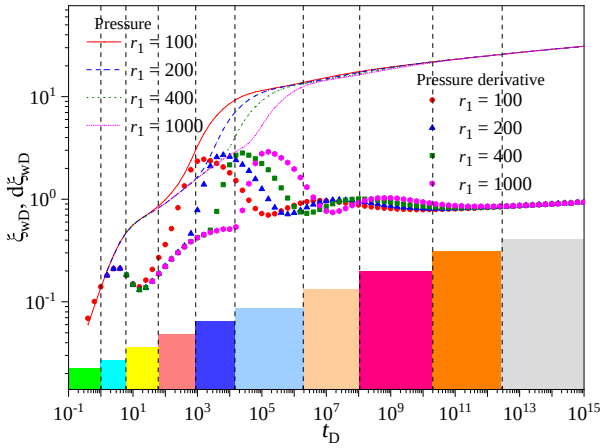

Fig. 7. Effect of dissociated-area radius on multi-branch well's pressure response.

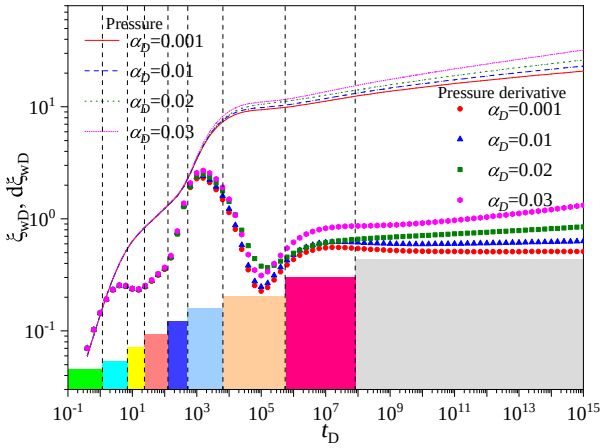

Fig. 9. Effect of the stress-sensitive coefficient on multi-branch well's response.

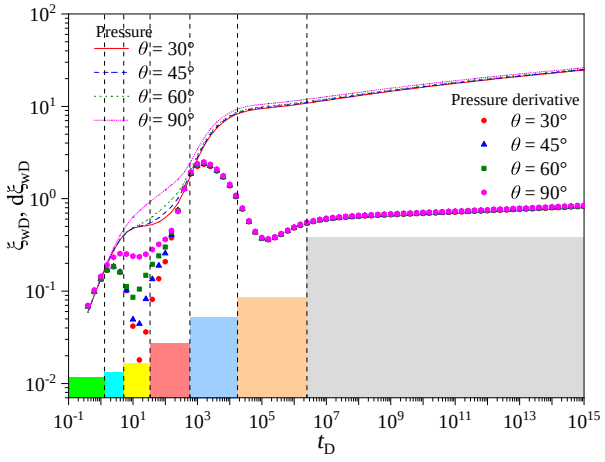

Fig. 8. Effect of branch angle on multi-branch well's pressure response.

In contrast, the composite-effect, dissociated, transitional, and improvement flow regimes are governed by NGH properties.

(d)Effect of stress-sensitive coefficient

Fig. 9 illustrates the effect of the stress-sensitive coefficient on the pressure derivative. The stress-sensitive coefficient affects the change of permeability with stress. The flow regimes affected include composite-effect, dissociated, transitional, improvement, and stress-sensitive effect regimes. As the dimensionless stress-sensitive coefficient increases, the pressure derivative increases during the stress-sensitive effect flow regime.

5. Case study

The Pearl River Mouth Basin (Fig. 10) is the largest oil and gas basin in the South China Sea. Geological exploration evidence demonstrates that several NGH orebodies are distributed in the South China Sea; we selected the Baiyun Sag area as the test area (Cheng et al., 2020; Jin et al., 2022; Qin et al., 2022). Well logs (Fig. 10(b)) and core analysis data show that the distance from the overlying strata to the seabed is 1495 m. From top to bottom, the NGH reservoirs in the test region can be divided into three sets of strata, including solid-gas hydrate, liquid water, and free methane gas. The lithology of NGH reservoirs in Fig. 11 is clayey siltstone (Li et al., 2018; Ye et al., 2020). The average median particle size of the sediment is about 12 μm. The mineral composition includes quartz feldspar (53%), carbonate (18%), and clay minerals represented by montmorillonite and illite (26%-30%), as Fig. 11 shows. Porosity ranges from 32% to 35%. The average permeability ranges from 1.5 to 7.4 mD. The NGH reservoir below 1,530 m, considered the region with the most significant potential for gas production, contains three phases: solid NGH, free hydrocarbon gas, and liquid water. Temperatures and pressures in this region are closest to the NGH phase equilibrium curve, which is suitable for recovering NGH (Li et al., 2018). Methane accounts for more than 99% of produced gas in hydrate-bearing cores.

Through 2022, the China Geological Survey conducted two production tests of NGH from the Shenhu area in the South China Sea. Operators use an offshore drilling platform (e.g., Blue Whale 1) for NGH drilling operations. Due to the unique structure of multi-branch wells and the potential cost, companies have regarded enhancing NGH production as an add-on option (Wilson et al., 2011). The typical parameters of the reservoir, gas hydrate, and multi-branch wells in the Shenhu area of the South China Sea are used as model inputs, as given in Table 2. Using these parameters, the synthetic pressure profiles for multi-branch wells are generated (Fig. 12). With certain combinations of parameters, many of the theoretical flow regimes may appear in actual test data from NGH reservoirs. However, the prominent dissociated regime masks the later transitional and improvement flow regimes. Due to test-time constraints, earlier flow regimes are more likely to exist in the actual data.

6. Conclusions

This study developed a semi-analytical multi-branch well model for NGH accumulations. The innovations include a new multi-branch well model of NGH and a procedure to identify

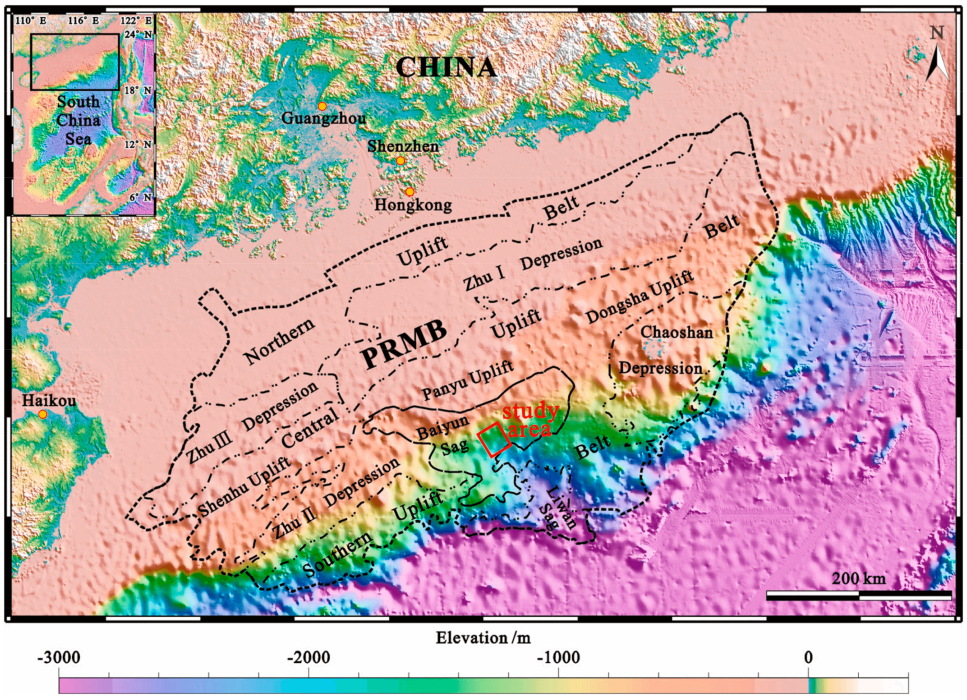

(a)

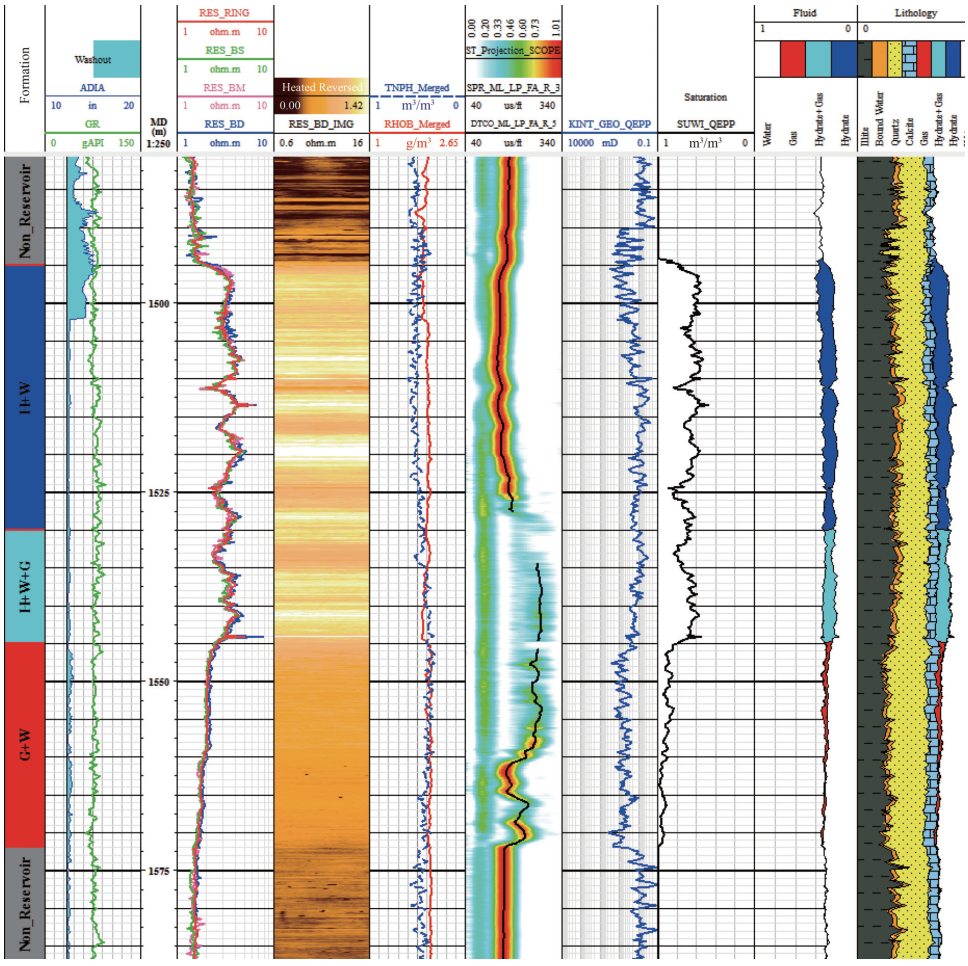

(b)

Fig. 10. (a) Gas hydrate study area location map in the Shenhu area of the South China Sea, (b) log data from a production test well in the Shenhu area (modified from Li et al., (2018); Cheng et al., (2020)). PMRB refers to the Pearl River Mouth Basin.

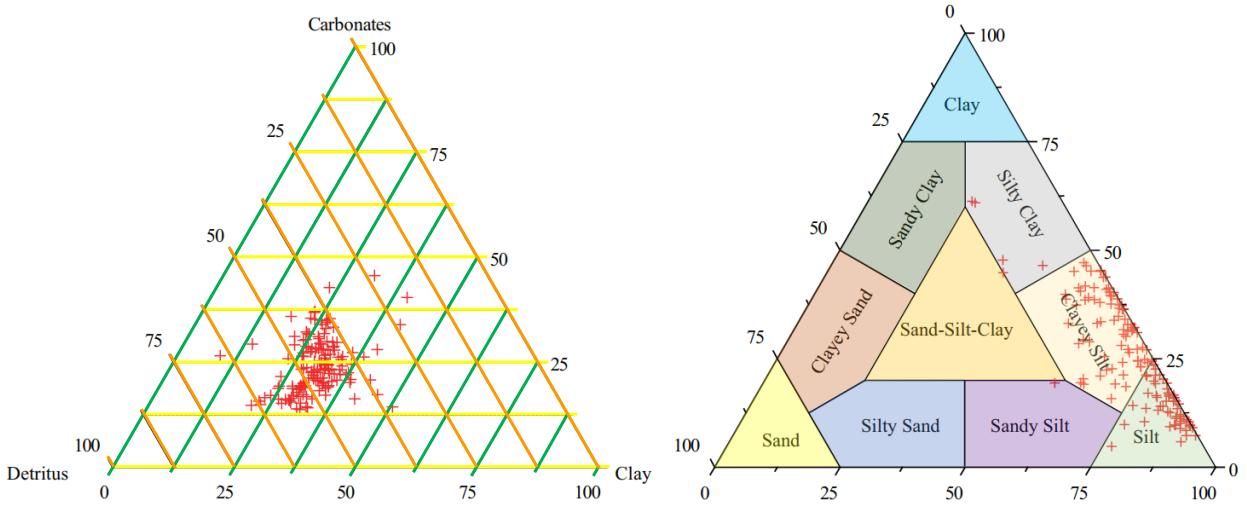

Fig. 11. Mineralogy and lithology of sediments in gas hydrate study area (modified from Li et al., (2018)).

Table 2. Gas hydrate, formation, and well properties in the case study of the Shenhu area (Parameter sources include Li et al. (2010) and Jin et al. (2022)).

Parameter	Value	Unit
Underburden thickness	30	m
Formation thickness	22	m
Initial dissociated region radius	1000	m
Initial pressure	13.83	MPa
Initial saturation	44	%
Temperature	287.31	K
Grain density	2600	kg/m^3
Porosity	37.3	%
Permeability	2.38	mD
Branch length	250	m
Number of branches	2	-
Bottom hole pressure	7	MPa
NGH composition 100%	CH4	-
NGH volume factor	0.01	-
NGH dissociation coefficient	2×10^{-4}	-
Compressibility	2×10^{-4}	-
Stress sensitivity coefficient	1.45	MPa$^{-1}\cdot$s

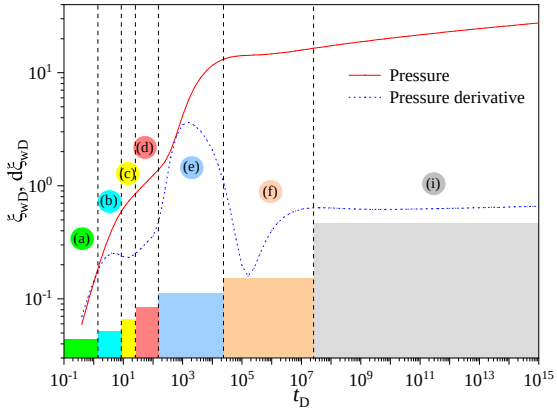

Fig. 12. Synthetic transient pressure profiles for multi-branch well testing in the Shenhu NGH area of the South China Sea.

the typical flow regimes in the pressure profiles of multi-branch wells in the South China Sea. Some conclusions from this study include the following:

1) The typical flow regimes of pressure profiles from well tests in multi-branch wells in NGH include wellbore storage and skin effects, vertical-radial, linear, pseudo-radial, composite-effect, dissociated, transitional, improvement, and stress-sensitive effect flow regimes. A multi-branch well structure controls the vertical radial flow and the linear flow regimes. The composite-effect, dissociated, transitional, and improvement flow regimes are governed by NGH formation properties.
2) As the dissociation coefficient increases, the amount of dissociated natural gas also increases, and the conversion process of NGH to natural gas is instantaneous. The reservoir behaves as a homogeneous reservoir. The radius of the dissociated area is proportional to production time and the duration of the composite-effect, dissociated, transitional, and improvement regimes. As the properties of the outer region are fixed benchmarks, the flow capacity in the inner zone increases with increases in mobility ratio. The derivative also increases as the mobility ratio increases.
3) The branch angle correlates positively with the derivatives during vertical radial and linear flow regimes. This derivative change caused by branch angle peaks during vertical radial flow and gradually weakens in the later linear flow regime. The influence of the stress-sensitive coefficient on the pressure behaviors is concentrated in the stress-sensitive effect regime. Derivatives during the stress-

sensitive effect period increase as the stress-sensitive coefficient increases.

7. Future Work

This paper presents the pressure solution and well-test model for multi-branch wells producing from NGH accumulations. The parameters obtained from well-test analysis can be used to predict production match history. The proposed model has limitations, including single-phase flow and laminar flow. The flow of formation water and the flow pattern changes caused by the injection of a heated fluid to dissociate NGH reserves are ignored. Thus, our subsequent research will focus on the effects of gas-water two-phase flow and turbulent flow regimes in predicting production.

Acknowledgements

We are very grateful to everyone who contributed to this work. This study received funding support from the National Natural Science Foundation of China (No. 12202042), China Postdoctoral Science Foundations (No. 2021M700391), and Fundamental Research Funds for the Central Universities (Nos. QNXM20220011, FRF-TP-22-119A1).

Conflict of interest

The authors declare no competing interest.

References

Blasingame, T. A., Lee, W. J. The variable-rate reservoir limits testing of gas wells. Paper SPE 17708 Presented at SPE Gas Technology Symposium, Dallas, Texas, 13-15 June, 1988.

Blasingame, T. A., McCray, T. L., Lee, W. J. Decline curve analysis for variable pressure drop/variable flowrate systems. Paper SPE 21513 Presented at SPE Gas Technology Symposium, Houston, Texas, 22-24 January, 1991.

Bourdet, D., Ayoub, J. A., Plrard, Y. M. Use of pressure derivative in well-test interpretation. SPE Formation Evaluation, 1989, 4(2): 293-302.

Cai, J., Xia, Y., Lu, C., et al. Creeping microstructure and fractal permeability model of natural gas hydrate reservoir. Marine and Petroleum Geology, 2020a, 115: 104282.

Cai, J., Xia, Y., Xu, S., et al. Advances in multiphase seepage characteristics of natural gas hydrate sediments. Chinese Journal of Theoretical and Applied Mechanics, 2020b, 52(1): 208-223. (in Chinese)

Chen, Z., Li, D., Zhang, S., et al. A well-test model for gas hydrate dissociation considering a dynamic interface. Fuel, 2022, 314: 123053.

Cheng, C., Jiang, T., Kuang, Z., et al. Characteristics of gas chimneys and their implications on gas hydrate accumulation in the Shenhu area, northern South China Sea. Journal of Natural Gas Science and Engineering, 2020, 84: 103629.

Chu, H., Ma, T., Gao, Y., et al. A composite model based on semi-analytical method for multiwell horizontal pad with stimulated reservoir volume. Journal of Petroleum Science and Engineering, 2022, 217: 110910.

Chu, H., Ma, T., Zhu, W., et al. A novel semi-analytical monitoring model for multi-horizontal well system in large-scale underground natural gas storage: Methodology and case study. Fuel, 2023, 334: 126807.

Dincer, I., Acar, C. A review on clean energy solutions for better sustainability. International Journal of Energy Research, 2015, 39(5): 585-606.

Gielen, D., Boshell, F., Saygin, D., et al. The role of renewable energy in the global energy transformation. Energy Strategy Reviews, 2019, 24: 38-50.

Goel, N., Wiggins, M., Shah, S. Analytical modeling of gas recovery from in situ hydrates dissociation. Journal of Petroleum Science and Engineering, 2001, 29(2): 115-127.

Gringarten, A. C., Ramey, H. J., Raghavan, R. Unsteady-state pressure distributions created by a well with a single infinite-conductivity vertical fracture. Society of Petroleum Engineers Journal, 1974, 14(4): 347-360.

He, Y., Cheng, S., Li, S., et al. A semianalytical methodology to diagnose the locations of underperforming hydraulic fractures through pressure-transient analysis in tight gas reservoir. SPE Journal, 2017, 22(3): 924-939.

Hepburn, C., Qi, Y., Stern, N., et al. Towards carbon neutrality and China's 14th Five-Year Plan: clean energy transition, sustainable urban development, and investment priorities. Environmental Science and Ecotechnology, 2021, 8: 100130.

Hong, H., Pooladi-Darvish, M., Bishnoi, P. R. Analytical modeling of gas production from hydrates in porous media. Journal of Canadian Petroleum Technology, 2003, 42(11): 45-56.

Hou, J., Zhao, E., Liu, Y., et al. Pressure-transient behavior in class III hydrate reservoirs. Energy, 2019, 170: 391-402.

Jin, G., Peng, Y., Liu, L., et al. Enhancement of gas production from low-permeability hydrate by radially branched horizontal well: Shenhu Area, South China Sea. Energy, 2022, 253: 124129.

Kushwaha, O. S., Meshram, S. B., Bhattacharjee, G., et al. Molecular Insights about Gas Hydrate Formation. in Advances in Spectroscopy: Molecules to Materials, edited by O. S. Kushwaha, S. B. Meshram, G. Bhattacharjee, et al. Springer, Singapore, 2019: 311-322.

Kvenvolden, K. A., Rogers, B. W. Gaia's breath-global methane exhalations. Marine and Petroleum Geology, 2005, 22(4): 579-590.

Lee, J. Well Testing, Society of Petroleum Engineers, 1982.

Lee, J., Rollins, J. B., Spivey, J. P. Pressure transient testing (eBook). SPE Textbook Series, 2003.

Li, Y., Liu, L., Jin, Y., et al. Characterization and development of natural gas hydrate in marine clayey-silt reservoirs: A review and discussion. Advances in Geo-Energy Research, 2021, 5(1): 75-86.

Li, G., Moridis, G. J., Zhang, K., et al. Evaluation of the gas production potential of marine hydrate deposits in the

Shenhu Area of the South China Sea. Paper OTC 20548 Presented at Offshore Technology Conference, Houston, Texas, 3-6 May, 2010.

Li, J., Ye, J., Qin, X. et al. The first offshore natural gas hydrate production test in South China Sea. China Geology, 2018, 1(1): 5-16.

Lu, C., Qin, X., Ma, C., et al. Investigation of the impact of threshold pressure gradient on gas production from hydrate deposits. Fuel, 2022, 319: 123569.

Myshakin, E. M., Ajayi, T., Anderson, B. J., et al. Numerical simulations of depressurization-induced gas production from gas hydrates using 3-D heterogeneous models of L-Pad, Prudhoe Bay Unit, North Slope Alaska. Journal of Natural Gas Science and Engineering, 2016, 35: 1336-1352.

Nair, V. C., Gupta, P., Sangwai, J. S. Gas hydrates as a potential energy resource for energy sustainability, in Sustainable Energy Technology and Policies, edited by S. De, S. Bandyopadhyay, M. Assadi, et al. Springer, Singapore, pp. 265-287, 2018.

Nakajima, C., Ouchi, H., Tamaki, M., et al. Sensitivity and uncertainty analysis for natural gas hydrate production tests in Alaska. Energy & Fuels, 2022, 36(14): 7434-7455.

Newell, R., Raimi, D., Aldana, G. Global energy outlook 2019: the next generation of energy. Resources for the Future, 2019, 1: 8-19.

Ozkan, E., Raghavan, R. New solutions for well-test-analysis problems: Part 1-analytical considerations. SPE Formation Evaluation, 1991, 6(3): 359-368.

Pedrosa Jr, O. A. Pressure transient response in stress-sensitive formations. Paper SPE 15115 Presented at SPE California Regional Meeting, Oakland, California, 2-4 April, 1986.

Qin, X., Lu, C., Wang, P., et al. Hydrate phase transition and seepage mechanism during natural gas hydrates production tests in the South China Sea: A review and prospect. China Geology, 2022, 5: 201-217.

Roostaie, M., Leonenko, Y. Analytical investigation of gas production from methane hydrates and the associated heat and mass transfer upon thermal stimulation employing a coaxial wellbore. Energy Conversion and Management, 2020, 209: 112616.

Shaibu, R., Sambo, C., Guo, B., et al. An assessment of methane gas production from natural gas hydrates: Challenges, technology and market outlook. Advances in Geo-Energy Research, 2021, 5(3): 318-332.

Spivey, J. P., Lee, W. J. New solutions for pressure transient response for a horizontal or a hydraulically fractured well at an arbitrary orientation in an anisotropic reservoir. Paper SPE 49236 Presented at SPE Annual Technical Conference and Exhibition, New Orleans, Louisiana, 27-30 September, 1998.

Spivey, J. P., Lee, W. J. Applied Well Test Interpretation. Society of Petroleum Engineers, 2013.

Stehfest, H. Algorithm 368: Numerical inversion of Laplace transforms [D5]. Communications of the ACM, 1970, 13(1): 47-49.

Sun, X., Nanchary, N., Mohanty, K. K. 1-D modeling of hydrate depressurization in porous media. Transport in Porous Media, 2005, 58(3): 315-338.

Tsimpanogiannis, I. N., Lichtner, P. C. Parametric study of methane hydrate dissociation in oceanic sediments driven by thermal stimulation. Journal of Petroleum Science and Engineering, 2007, 56(1-3): 165-175.

Tsypkin, G. G. Mathematical models of gas hydrates dissociation in porous media. Annals of the New York Academy of Sciences, 2000, 912(1): 428-436.

Uddin, M., Coombe, D., Law, D., et al. Numerical studies of gas hydrate formation and decomposition in a geological reservoir. Journal of Energy Resources Technology, 2008, 130(3): 032501.

Van Everdingen, A. F., Hurst, W. (1949). The application of the Laplace transformation to flow problems in reservoirs. Journal of Petroleum Technology, 1949, 1(12): 305-324.

Wei, C., Liu, Y., Deng, Y., et al. Temperature Transient Analysis of Naturally Fractured Geothermal Reservoirs. SPE Journal, 2022, 27(5): 2723-2745.

Wilson, S. J., Hunter, R. B., Collett, T. S., et al. Alaska North Slope regional gas hydrate production modeling forecasts. Marine and Petroleum Geology, 2011, 28(2): 460-477.

Wu, Z., Yang, S., Liu, W., et al. Permeability analysis of gas hydrate-bearing sand/clay mixed sediments using effective stress laws. Journal of Natural Gas Science and Engineering, 2022, 97: 104376.

Xiao, C., Tian, L. Modelling of fractured horizontal wells with complex fracture network in natural gas hydrate reservoirs. International Journal of Hydrogen Energy, 2020, 45(28): 14266-14280.

Yan, C., Ren, X., Cheng, Y., et al. Geomechanical issues in the exploitation of natural gas hydrate. Gondwana Research, 2020, 81: 403-422.

Ye, J., Qin, X., Xie, W., et al. The second natural gas hydrate production test in the South China Sea. China Geology, 2020, 3: 197-209.

Ye, H., Wu, X., Li, D., et al. Numerical simulation of productivity improvement of natural gas hydrate with various well types: Influence of branch parameters. Journal of Natural Gas Science and Engineering, 2022: 104630.

Ye, H., Wu, X., Guo, G., et al. Application of the enlarged wellbore diameter to gas production enhancement from natural gas hydrates by complex structure well in the Shenhu Sea area. Energy, 2023, 264: 126025.

Zhang, P., Tian, S., Zhang, Y., et al. Numerical simulation of gas recovery from natural gas hydrate using multi-branch wells: A three-dimensional model. Energy, 2021, 220: 119549.

Zhang, P., Zhang, Y., Zhang, W., et al. Numerical simulation of gas production from natural gas hydrate deposits with multi-branch wells: Influence of reservoir properties. Energy, 2022, 238: 121738.

Appendix A. Dimensionless variables

The dimensionless pressure for the dissociated NGH region is:

$$\Psi_{1D} = \frac{k_i h\left(\Psi_i - \Psi_1\right)}{3.684 \times 10^{-3} \mu^2 B_H q_{sc} Z} \tag{A1}$$

where Ψ is:

$$\Psi = \int_0^p \frac{2p}{\mu Z} dp \tag{A2}$$

The dimensionless pressure for the non-dissociated region is:

$$\Psi_{2D} = \frac{k_i h\left(\Psi_i - \Psi_2\right)}{3.684 \times 10^{-3} \mu^2 B_H q_{sc} Z} \tag{A3}$$

Dimensionless time is:

$$t_D = \frac{3.6 k_i t}{\mu \varphi C_t L^2} \tag{A4}$$

where L is the reference length.

Dimensionless wellbore storage coefficient is:

$$C_D = \frac{C}{2\pi \varphi C_t h L^2} \tag{A5}$$

Mobility ratio is:

$$M_{12} = \frac{\left(\frac{k_i}{\mu}\right)_1}{\left(\frac{k_i}{\mu}\right)_2} \tag{A6}$$

Diffusivity ratio of inner region and outer region is:

$$W_{12} = \frac{(\varphi C_t)_1}{(\varphi C_t)_2} \tag{A7}$$

Dimensionless radial distance is:

$$r_D = \frac{r}{L} \tag{A8}$$

Improved permeability modulus is:

$$\gamma = \frac{\alpha \mu Z}{2p} \tag{A9}$$

Stress-sensitive coefficient is:

$$\gamma_D = \frac{3.684 \times 10^{-3} p_{sc} q_{sc} T}{k_i T_{sc} h} \gamma \tag{A10}$$